ChemPubSoc Europe

DOI: 10.1002/cctc.201701517

CHEMCATCHEM Full Papers

Unraveling the Nature of the Catalytic Power of Fluoroacetate Dehalogenase

Sebastián Miranda-Rojas,*[a] Israel Fernández,[b] Johannes Kästner,[c] Alejandro Toro-Labbé,[d] and Fernando Mendizábal[e]

Fluoroacetate dehalogenase is able to cleavage a carbon–fluoride bond, the strongest carbon–halogen bond in nature, in a process initiated by a S_N2 reaction. The role of the enzyme machinery and particularly of the halogen pocket in the S_N2 reaction is thoroughly explored by using state-of-the-art computational tools. A comparison between the non-catalyzed versus enzyme-catalyzed reaction, as well as with a mutant of the enzyme (Tyr219Phe), is presented. The energy barrier changes are rationalized by means of reaction force analysis and the activation strain model coupled with energy decomposition analysis. The catalysis is in part caused by the reduction of structural work from bringing the reactant species towards the proper reaction orientation, and the reduction of the electrostatic repulsion between the nucleophile and the substrate, which are both negatively charged. In addition, catalysis is also driven by an important reduction of the electronic reorganization processes during the reaction, where Tyr from the halogen pocket acts as a charge acceptor from the S_N2 reaction axis therefore reducing the electronic steric repulsion between the reacting parts.

Introduction

The degradation of halogenated compounds has become a relevant environmental issue,[1–3] where fluorinated compounds are the most difficult to eliminate owing to the relatively high strength of the carbon–fluorine bond.[4] This makes the dehalogenation process much harder to accomplish compared with compounds possessing heavier halogen atoms. Sodium fluoroacetate (FAc) is a fluorinated α-haloacid present in plants endemic to Australia, Africa, and Central America, and is highly poisonous for mammals,[5–7] which is an important problem for the livestock industry. In nature, fluoroacetate dehalogenase (FAcD) is the enzyme responsible for its degradation into harmless glycolate through an hydrolytic dehalogenation reaction.[8] The widely accepted mechanism of the defluorination of FAc consists of a two-stage process (Scheme 1). It starts with the nucleophilic attack (S_N2) to the α-carbon (αC) of the substrate by an aspartate residue, causing the dissociation of the carbon–fluorine bond (αC–F) and the formation of an ester intermediate (step A). Then, a water molecule activated by an aspartate–histidine (Asp-His) pair hydrolyzes the ester bond with the subsequent generation and release of the reaction product (step B).

The architecture of the catalytic site of FAcD includes the halogen pocket depicted in Scheme 1, which consists of three residues that coordinate the halogen, namely histidine (His), tryptophan (Trp), and tyrosine (Tyr). Experimental evidence suggests that the mutation of Trp in FAcD results in the inactivation of the enzyme.[10] Computational studies have been carried out in haloalkane dehalogenase (HAD), which catalyzes the dehalogenation of dichloroethane through the hydrolytic cleavage of the carbon–chlorine bond. These studies have highlighted the relevance of the electrostatic preorganization of the binding site in the stabilization of the corresponding transition state.[11,12] In addition, it has been proven that other possible explanations such as the so-called *near attack conformation* (NAC) mechanism[13–15] have only a minor contribution to the reduction of the barrier induced by several enzymes.[11,16,17] Unfortunately, the physical factors that govern the catalysis and their relationship with the chemical structure of the enzyme are not fully understood so far, which hampers the design of new, more efficient catalysts.

Two recent theoretical studies based on the crystal structure of the FAcD FA1 (*Burkholderia sp.*) performed by Yoshizawa

[a] *Prof. Dr. S. Miranda-Rojas*
Departamento de Ciencias Químicas
Facultad de Ciencias Exactas
Universidad Andres Bello, Av. República 275, Santiago (Chile)
E-mail: sebastian.miranda@unab.cl

[b] *Prof. Dr. I. Fernández*
Departamento de Química Orgánica I and Centro de Innovación en Química Avanzada (ORFEO-CINQA)
Facultad de Ciencias Químicas
Universidad Complutense de Madrid, 28040-Madrid (Spain)

[c] *Prof. Dr. J. Kästner*
Institut für Theoretische Chemie
Universität Stuttgart
Pfaffenwaldring 55, 70569 Stuttgart (Germany)

[d] *Prof. Dr. A. Toro-Labbé*
Laboratorio de Química Teórica Computacional, Facultad de Química
Pontifica Universidad Católica de Chile
Av. Vicuña Mackenna 4860, Macul, Santiago (Chile)

[e] *Prof. Dr. F. Mendizábal*
Departamento de Química, Facultad de Ciencias
Universidad de Chile
Las Palmeras 3425, Ñuñoa, Santiago (Chile)

Supporting information and the ORCID identification number(s) for the author(s) of this article can be found under https://doi.org/10.1002/cctc.201701517.

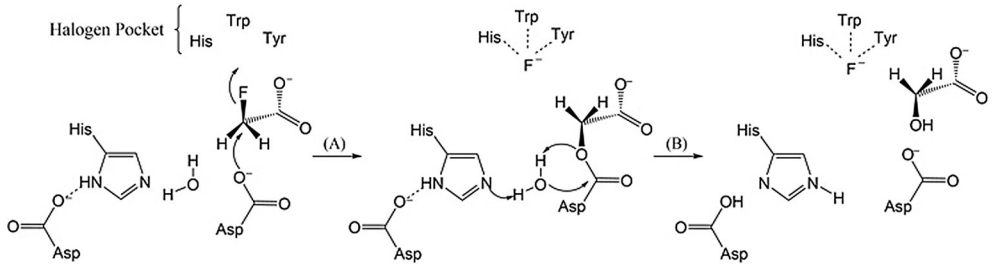

Scheme 1. Proposed reaction mechanism for fluoroacetate dehalogenase. The first step (A) corresponds to the S_N2 reaction, which is the focus of this study. The second step (B) involves the hydrolytic cleavage of the ester intermediate. Adapted from reference [9].

et al.,[18,19] confirm the notion that the most important factor for the reduction of the activation barrier towards the αC–F bond cleavage is the interaction of the fluorine with the halogen pocket. It was suggested that the most important residue from the halogen pocket in reducing the energy barrier is the Tyr, which exhibits the shortest interaction with fluoride after αC–F bond cleavage. These results reinforce the relevance of the Tyr in the S_N2 step of the reaction cycle. Nevertheless, the mechanism by which Tyr reduces the energy barrier of the S_N2 elementary step still needs to be explored to obtain a complete picture of the halogen pocket inner working. Subsequent studies were carried out by Pai et al.,[9] in which they crystallized a FAcD from *Rhodopseudomonas palustris* (RPA1163) in complex with the substrate (FAc), and arrived at similar conclusions. They also performed steady-state kinetic measurements for several mutants of RPA1163, providing insights into the reactivity. Among these, the mutation of Tyr219 to phenylalanine (Tyr219Phe; numbering according to PDB ID 3R3V from *Rhodopseudomonas palustris*)[9] from the halogen pocket led to a release of the steric constraint in the binding site, accompanied with the loss of an interaction point for the halogen. Based on this crystal structure, Zhang et al.[20] carried out a quantum mechanical (QM)/molecular mechanics (MM) study of FAcD by using a scheme involving several snapshots to calculate the barrier of the reaction. They found that the reaction barrier spreads over a range from 9.5 to 21.5 kcal mol^{-1}, depending on the snapshot used for the calculation. Also, they pointed out the correlation existing between the angle formed by (Asp110)O-αC-F in the reactant state and the reaction barrier, where angles closer to the theoretical 180° may involve lower energy barriers.

Considering all the previous studies mentioned above, herein, we will unravel the source of the catalytic power provided by the enzymatic machinery for the initial S_N2 elementary step, which holds information that may lead to the efficient dehalogenation of other compounds. First, we transversely dissected the reaction coordinate into three regions, each one dominated either by structural or electronic contributions as revealed by the reaction force analysis (RFA).[21–23] Afterwards, to gain more insight into the physical factors involved in the S_N2 reaction, we used the activation strain model coupled to the energy decomposition analysis (ASM-EDA) along the entire reaction coordinate. To this end, we have performed an extensive computational study by means of DFT by using the quantum chemical cluster approach to model the catalytic site and the substrate of the reaction. In addition, we also present a detailed study of the impact of the Tyr219Phe mutation on the S_N2 reaction mechanism within the scope of the RFA and ASM-EDA. This represents a paramount opportunity to explore the role of the steric effect provided by the binding site, together with the relevance of the electronic reorganization processes involved in this type of catalysis. The comparative analysis between the native enzyme and the impaired mutant will allow us to understand the inner working of the enzymatic machinery, providing new chemical insights to support the development of new environmental technologies focused on bioremediation.

Results and Discussion

The analysis of the crystal structure 3R3V indicates possible hydrogen bonds between TyrOH and F or O atoms of FAc. The TyrO···O distance is 2.74 Å whereas the TyrO···F distance is 3.28 Å, indicating a preference for the TyrOH···O hydrogen bond. Figure 1 displays the time evolution of the distances of TyrOH···O and TyrOH···F during the MD simulation. These two

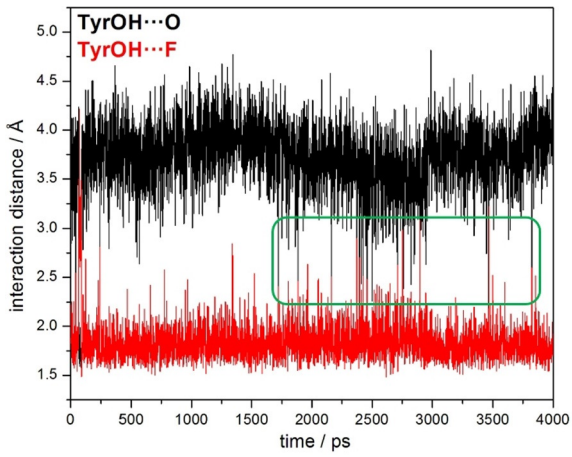

Figure 1. Plot of the interaction distances between the hydrogen from the hydroxyl group of Tyr219 with the carboxylic oxygen (black) and with the fluorine atom (red), both from FAc. Enclosed in the green box is the region where some snapshots are found in a similar conformation as the crystal structure (PDB code: 3R3V), namely a short Tyr···O interaction and a long Tyr···F interaction.

geometric parameters define the main conformations adopted along the production trajectory, indicating the feasibility of a TyrOH···O configuration. The results show that the TyrOH···O interaction is rare (green rectangle in Figure 1). At variance, the TyrOH···F configuration, which we will later identify as catalytically active, dominates. Selecting those snapshots with TyrOH···O shorter than 2.0 Å and simultaneously TyrOH···F larger than 2.5 Å, we found only 28 structures out of 4000 from our sampling, meaning that only 0.7% of the production trajectory had access to that conformation. The selection criterion was defined according to the interaction distances predicted after adding the hydrogen atoms to the crystal structure, resulting in 1.74 Å and 2.28 Å for TyrOH···O and TyrOH···F, respectively; but providing a certain range of flexibility to these magnitudes to increase the population number. It is noticed from Figure 1 that in general the TyrOH···F interaction is shorter than TyrOH···O and it varies between a short range of distances, whereas TyrOH···O seems to be less stable. From these conformations, we selected our snapshot for further studies by following the criteria detailed in the Computational Details section.

The calculated energy barrier for the wild-type model (**R1**) obtained from the selected snapshot was of 5.3 kcal mol^{-1}, close to the values previously reported by means of QM/MM methods (4.3 kcal mol^{-1}).[18] Our results are also in agreement with the structural correlation proposed by Zhang et al.[20] occurring between the angle formed by (Asp110)O-αC-F in the reactant state and the reaction barrier, where the angle of the reactant state of **R1** was 177°, close to the theoretical value of 180°. This explains the low energy barrier obtained from our careful snapshot selection. An additional explanation for the low energy barrier compared with that calculated by Zhang et al. seems to be associated with the method of choice for the energy analysis. After calculating the energy barrier of **R1** with our geometries at the ri-MP2, SCS-ri-MP2, and SOS-ri-MP2 levels of theory and by using their same basis set (cc-pVTZ), we obtained values of 7.1, 8.4, and 9.1 kcal mol^{-1}, which are higher and closer to the values obtained in that work. Nevertheless, for the purposes of this work, B3LYP is still a good choice as it provides reliable geometries as previously tested,[18–20] and accurate enough energetics for S_N2 reactions,[24,25] as the one studied in this work. All the calculated energy barriers ($\Delta E^{\neq}$), reaction works (W_i), and reaction energies (ΔE°) are listed in Table 1, whereas the reaction force profiles are shown in Figure S2 (in the Supporting Information). We defined the 5.3 kcal mol^{-1} as our reference value for further comparative analysis. This energy barrier represents a tremendous decrease compared with the 31.1 kcal mol^{-1} computed for the non-catalyzed reaction in implicit aqueous solvent at the same level of theory.[26] To rationalize this significant energy decrease, RFA was applied next.

Table 1. Reaction energies, energy barriers, and reaction works associated with reaction models **R1**–**R5**.[a]

Model	$\Delta E^{\neq}$	W_1	W_2	W_3	W_4	ΔE^{0}
R0[b]	31.1	20.7	10.5	−4.2	−11.8	15.1
R1	5.3	3.8	1.5	−10.6	−12.6	−17.9
R2	14.9	11.5	3.4	−6.0	−23.0	−14.1
R3	11.8	7.5	4.3	−6.5	−10.2	−4.9
R4	10.9	8.2	2.7	−8.8	−9.8	−7.7
R5	10.9	8.2	2.7	−9.3	−12.9	−11.3

[a] Values are in kcal mol^{-1}. **R1**: reference model; **R2**: from crystal structure; **R3**: Tyr219Phe mutant; **R4**: without His155; **R5**: without Trp156. W_1: non-spontaneous structural work; W_2: non-spontaneous electronic work; W_3: electronic relaxation, W_4: structural relaxation. [b] **R0** corresponds to the model for the non-catalyzed reaction, data previously published.[27]

Reaction force analysis of the barrier height

As can be seen in Table 1, for **R1** (wild-type enzyme) the structural changes (W_1) were the dominant factor as they contribute with approximately 72% of the total $\Delta E^{\neq}$. This value represents almost three times the contribution of the electronic reorganization (W_2) needed to reach the transition state (TS). Our previous studies on the non-catalyzed reaction in implicit water (model here designed as **R0**) showed a similar behavior, where the structural work was nearly twice as strong as the electronic work, with values of 20.7 and 10.5 kcal mol^{-1} for W_1 and W_2, respectively ($W_1/W_2 \approx 2$).[26] From these results, it is inferred that the structural work is a dominant feature of this particular reaction. The magnitude of W_1 for the enzyme-catalyzed reaction (**R1**) was 3.8 kcal mol^{-1}; 18.4% of the 20.7 kcal mol^{-1} calculated for the non-catalyzed reaction. This involved a reduction of W_1 and thus, of the energy barrier, of 16.9 kcal mol^{-1} with respect to the non-catalyzed reaction, highlighting the role of the enzyme in minimizing the conformational changes to begin with the O–αC bond formation.

Our starting geometry for the reactant state was the closest to the TS conformation from our molecular dynamics (MD), therefore, this result represents the highest probable reduction of the structural work possible to obtain from our conformational sampling. The reduction of the structural work also reflects the decrease of the electrostatic repulsion between the reacting parts and of the steric repulsion, where the latter will be further discussed in the ASM-EDA analysis section. The reduction of the electrostatic repulsion is achieved through the hydrogen-bonding network between the carboxylic moiety of FAc and Arg111/Arg114 pair, the importance of which has been previously shown,[20] together with the oxyanion hole, which stabilizes the charge from the nucleophile (Asp110).

The reduction of the electronic work (W_2) from 10.5 kcal mol^{-1} for the non-catalyzed reaction to the 1.5 kcal mol^{-1} calculated for **R1** also indicates a remarkable decrease of the electronic reorganization taking place during the reaction. This corresponds to 14.3% of the non-catalyzed energy barrier, showing a slightly higher reduction in the electronic reorganization than in the structural work. In this case, the electronic reorganization is associated with the two main chemical events of the reaction, namely the O–αC bond formation and the αC–F bond cleavage process. In addition, the stabilization of the incipient negative charge of the fluorine atom has proved to be an important factor for the reduction of the electronic work and thus, of the $\Delta E^{\neq}$ as previously reported.[26] In our previous

study, when FAc was protonated at its carboxylic moiety it was able to transfer that proton to the fluoride during the αC–F bond cleavage, decreasing the electronic work (W_2) from 10.5 to 5.1 kcal mol^{-1}. This indicated that the generation of the negative charge involves a huge amount of work of electronic nature. At this point, we suggest that for **R1** the factors responsible for the reduction of the electronic work are the assistance in the O–αC bond formation, the reduction of the αC–F bond strength through its stretching by the halogen pocket, and the stabilization of the nascent negative charge coming from the anion during the αC–F bond dissociation. In particular, the assistance of the O–αC bond formation is aided by the binding site by positioning the nucleophile and the substrate in a mutual orientation favoring an optimal orbital interaction necessary to start the electronic reorganization process. In general terms, these factors are probably connected to the preorganized electrostatic environment hypothesis, similar to the proposed mechanism for the binding site of HAD by Warshel et al.[11,12]

As explained in the Computational Details section, **R2** is a model directly obtained from the coordinates of the crystal structure, where Tyr219 is hydrogen bonded to one of the carboxylate oxygens from FAc instead of the fluorine at the reactant state as **R1**. Our calculations revealed that this reaction model suffered the largest increase of $\Delta E^{\neq}$, resulting in 14.9 kcal mol^{-1}, which is approximately three times the energy barrier obtained for **R1**. The magnitude of W_1 for **R2** was also three times higher than that of **R1**, pointing out that **R2** requires a huge amount of structural preparation before entering the transition state region (TSR). Meanwhile, in terms of the electronic work (W_2), **R2** needs to carry out more than twice the electronic activity performed by **R1**. Therefore, the reaction work analysis identifies a combined source for the increase in the reaction barrier, where the structural work was the most affected by this impaired conformation. Figure 2 shows that the TyrOH···O distance (dashed lines) remained almost unaltered

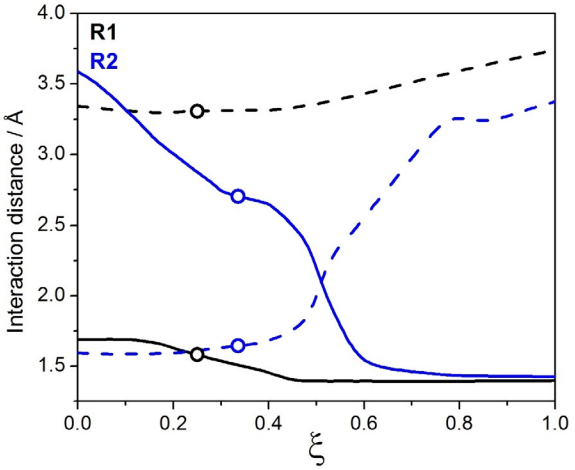

Figure 2. Interaction distances between TyrOH···F(FAc) (continuous line) and TyrOH···O(FAc) (dashed line) from **R1** (black) and **R2** (blue) along the reaction coordinate. For comparative purposes, we normalized the reaction coordinate (ξ). Circles denote the position of the TS.

until the TS was reached. This missing interaction with fluorine causes the lack of proper positioning of the halogen at the beginning of the reaction, which results in a larger translational movement of the halogen along the reactant region (RR) and the first half of the TSR.

Actually, as can be seen in Figure 3, at the TS the computed TyrOH···F distance for **R2** was 2.70 Å, much longer than the 1.58 Å observed for **R1**, showing that at this stage of the reaction the Tyr219 does not participate in the catalysis, leading to the large increase of the $\Delta E^{\neq}$.

According to these results, it can be concluded that the coordinates from the crystal structure do not represent a catalytically active complex, and that Tyr219 has to be within the interaction range of fluorine in the reactant state to then achieve the proper reduction of the energy barrier. From the study of **R2**, we found that adopting a different conformation than the active one (represented here by **R1**) involves an increase of almost three times the magnitude of $\Delta E^{\neq}$, with the structural work being the dominant contribution, also observed for **R1**. For **R2**, we found that the structural work was three times higher than the electronic work. This model in particular indicates that not only the integrity of the enzymatic machinery was necessary to achieve the catalytic process, but also the proper interactions between the halogen pocket and the fluorine. Here, the interaction of Tyr219 with the carboxylate oxygen from FAc triggered an increase in the structural demands to achieve the proper TS geometry, which even caused a slight increase in the interaction distance between the nucleophilic oxygen from Asp110 and the αC from **R2**, contributing to the increase of the $\Delta E^{\neq}$ (see Figure 3).

The $\Delta E^{\neq}$ resulting from the model of the Tyr219Phe mutant (**R3**) was 11.8 kcal mol^{-1}, showing an increase of 6.5 kcal mol^{-1} with respect to the wild-type **R1** system. According to experimental results,[9] this mutation impairs the catalytic activity of the enzyme, suggesting that this energy increase contributes to the disruption of the normal catalytic activity of the enzyme. According to the structural results presented in Figure 3, the mutation caused an increase of the interaction distance between (Asp110)O···αC of 0.13 Å. On the other hand, it also involved a slight decrease in the elongation of the αC–F bond of 0.04 Å, although this change was minor compared with the detrimental effect in the (Asp110)O···αC interaction distance. The shortest interaction distance between the halogen pocket residues and the fluorine atom at the TS was the Tyr219 (TyrOH···F 1.58 Å), as can be seen in Figure 3. Meanwhile, His155 and Trp156 present a comparable contribution inferred from the highly similar interaction distances with the fluorine atom (1.84 and 1.83 Å for Trp155 and His156, respectively). This is confirmed by the analysis of the TS of **R3**, where both Trp155 and His156 also interact with fluorine with highly similar interaction distances, but shorter than that observed for **R1**. Very likely, this occurs to compensate for the lack of stabilization provided by Tyr219. The role of the absence of Tyr219 in the increase of the energy barrier confirms the crucial role of a triad as the minimal structure for the halogen pocket in defluorination reactions. However, to test our proposal, we also designed two additional models with two residues each,

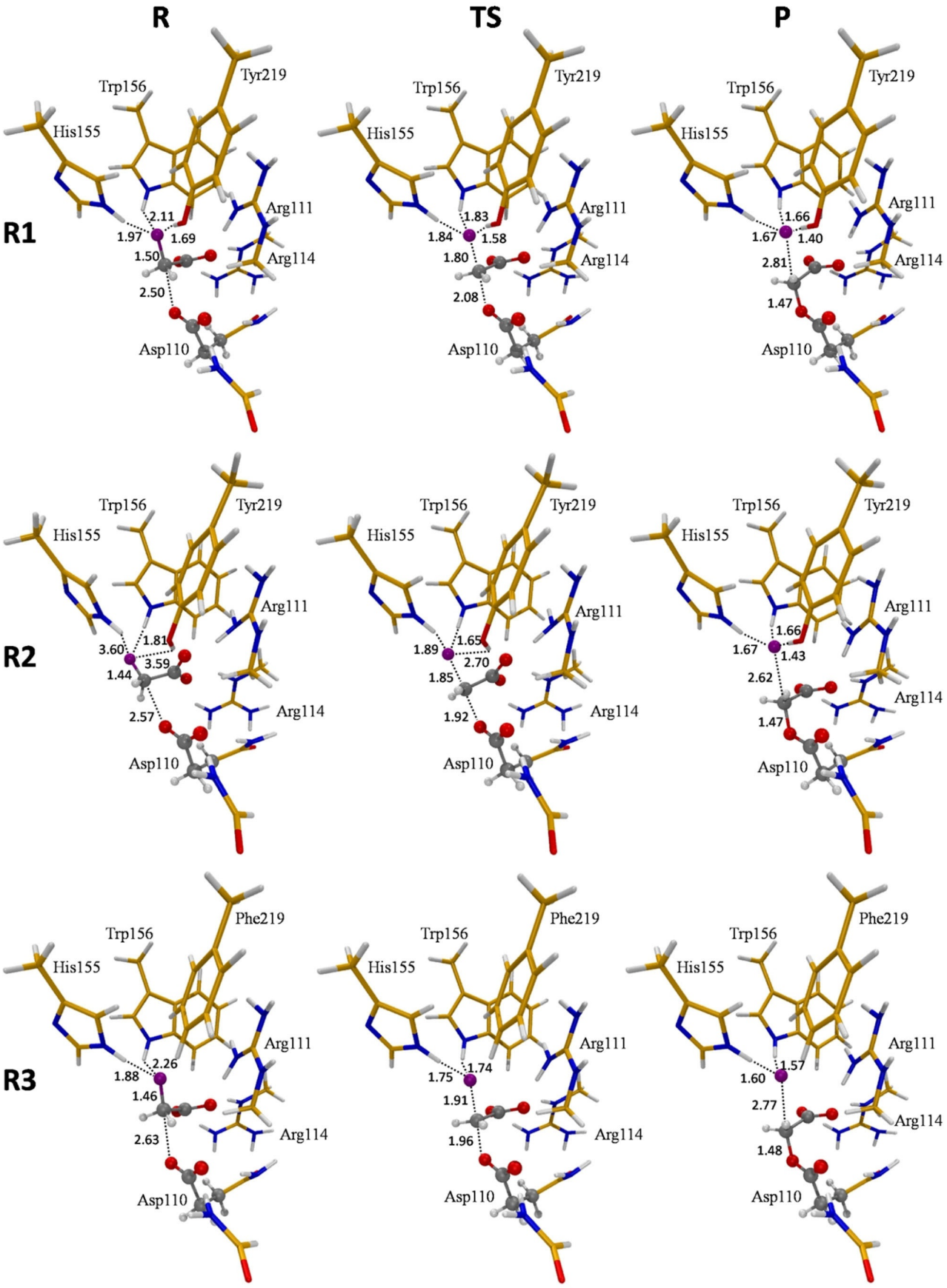

Figure 3. Main structural parameters of the geometries obtained for the reactant, TS, and product states of the reaction modeled by **R1**, **R2**, and **R3**. In orange are the carbon atoms from the enzymatic environment. In gray are the carbon atoms from the substrate and the fluorine atom is denoted in purple. Blue and red are reserved for the nitrogen and oxygen atoms, respectively.

one with a Tyr–Trp pair (**R4**), thus without the His, and the other with a Tyr–His pair (**R5**), missing the Trp. The geometries for the reactant, TS, and product states obtained for **R4** and **R5** are presented in Figure S1 (in the Supporting Information). Both **R4** and **R5** showed the same energy barrier (10.9 kcal mol^{-1}) exposing a slightly lower barrier compared with **R3**. In general, the three models showed an increase of the energy barrier close to a factor of two with respect to **R1**. These results demonstrate the importance of the three residues as part of the halogen pocket as a requirement for proper catalysis.

The magnitudes of the structural work (W_1) required by **R3** to pass through the RR and enter the TSR showed an increase of almost two times with respect to **R1**. This exposes that the absence of the OH group from Tyr219 causes an increase of the structural demands needed to reach the TSR. **R4** and **R5** needed slightly more than twice of the structural work required in **R1**. The slightly larger increase of W_1 for **R4** and **R5** compared with **R3** is probably due to the complete removal of His155 or Trp156, which increases the flexibility of the catalytic site during the reaction. Once in the TSR, the electronic reorganization process denoted by the values of W_2 starts to dominate the increase of the energy barrier. Here, **R3** showed an increase of three times the electronic work observed for **R1**, whereas the increase in the electronic work of **R4** and **R5** was only twice the magnitude calculated for **R1**. Then, the absence of His155 or Trp156 has a lower impact on the electronic reorganization. Our findings therefore suggest that Tyr219 is the most important residue in terms of the electronic reorganization to reach the TS configuration, and thus to overcome the reaction barrier. This indicates that the impairment caused by the mutation of Tyr219 is to a large extent the result of impairment in the electronic reorganization.

The increase in the structural work is partially explained by the fact that **R3**, **R4**, and **R5** showed larger distances between the nucleophilic oxygen from Asp and the αC from the substrate at the reactant state (see Figure 3). Thus, positioning the reactants in the proper orientation required for this transformation involved more structural work. However, the origin of the increase in the electronic reorganization is difficult to be unambiguously identified by means of the reaction force. For this reason, we complement these results with the ASM-EDA method (see below).

Reaction force analysis of product stabilization

The reaction energy (ΔE°) of **R1** was −17.9 kcal mol^{-1}, showing an exothermic behavior with a large stabilization of the products of the S_N2 reaction. **R2** also showed a large stabilization of the products with a ΔE° of −14.1 kcal mol^{-1}. After the TS point, Tyr219 from **R2** moves from interacting with the carboxylic oxygen from FAc towards the fluoride ion (see Figures 2 and 3), leading both **R1** and **R2** to adopt very similar conformations at the product state, thus explaining the obtained results. **R5** showed a ΔE° of −11.3 kcal mol^{-1}, whereas **R4** and **R3** were less exothermic, with ΔE° of −7.7 and −4.9 kcal mol^{-1}, respectively. The absence of the hydroxyl moiety from Tyr219 caused the largest loss of the stabilization provided by the catalytic site, highlighting the role of this residue as a component of the driving forces in charge of taking the reaction towards the products of the S_N2 reaction.

After crossing the TS point, each model is halfway in the formation process of the O–αC bond, which should be very similar in each model in terms of the electronic activity. Conversely, the αC–F bond cleavage and the coordination of the forming fluoride is different for each model, therefore the main differences in W_3 should be attributed to the latter process, meaning cleavage of the αC–F bond. The maximum electronic relaxation denoted by the value of W_3 was found for **R1** with −10.6 kcal mol^{-1}. The absence of Trp156 as part of the halogen pocket (**R5**) decreased this process by 1.3 kcal mol^{-1}, followed by **R4** with a decrease of 1.8 kcal mol^{-1}, thus indicating that neither His155 nor Trp156 have an indispensable role in the electronic relaxation process. On the other hand, the absence of the hydroxyl moiety from Tyr219 (**R3**) resulted in a decrease of W_3 of 4.1 kcal mol^{-1}, indicating that this residue is directly involved in the completion of the cleavage process of the αC–F bond.

The conformational relaxation in the binding site of the ester and the fluoride as products of the reaction is quantified by the value of W_4. In this case, the values for **R1** and **R5** were similar, hence exposing a minor role of Trp156 in the product region (PR). Similarly, the lack of Tyr219 or His155 modeled by **R3** and **R4**, respectively, only slightly affected the structural relaxation of the products of the reaction. These results point out that the structural relaxation is mostly focused on the final accommodation of the ester product in the binding site, a process that is similar among the models. This is because the residues needed for this accommodation, namely Asp110, Arg111, and Arg114, are present on every model. Consequently, we suggest that according to the magnitudes of W_3, the maximal stabilization and structural relaxation of the fluoride anion is reached at the end of the TSR, before entering the PR, whereas most of the ester accommodation takes places in the PR. **R2** represents a special case among the models studied, as it involved 23.0 kcal mol^{-1} of structural relaxation (W_4). As explained above, one of the largest conformational changes observed for **R2** involved the Tyr219, which after the TS started to move gradually towards the fluoride ion as denoted by the decrease in the TyrOH···F distance (see Figure 2). Then, along the PR it reached a similar interaction distance as that observed for **R1**.

ASM-EDA: Effect of the mutant Tyr219Phe on the barrier height

The ASM profiles of **R1** and **R3**, depicted in Figure 4a, showed the expected behavior, in the sense that the strain energy was the destabilizing contribution, whereas the interaction component corresponded to the stabilizing contribution to the barrier height. According to the fragmentation scheme used in this study, the behavior of the interaction energy directly reflects the bond formation process.

The comparison of the ASM diagrams computed for **R1** and **R3** showed that the ΔE_{strain} term is nearly identical along the

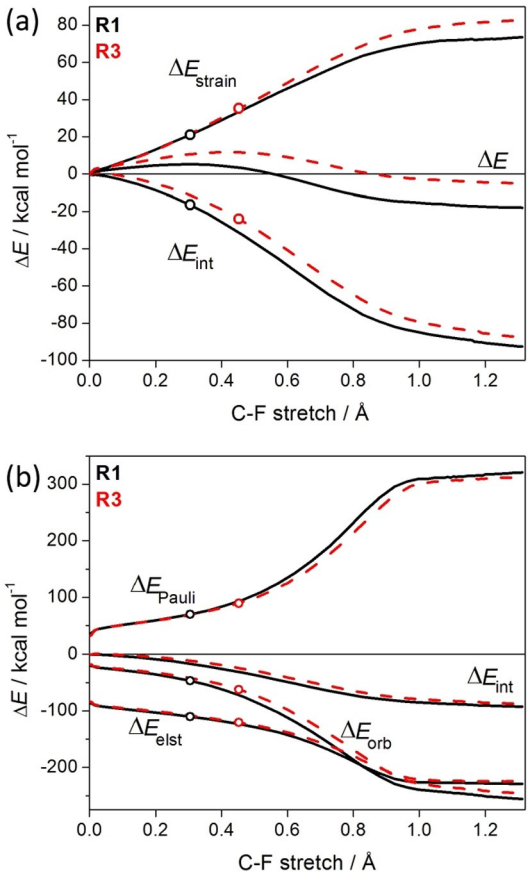

Figure 4. (a) Activation strain analysis and (b) EDA profiles calculated for the S_N2 reaction for the native enzyme modeled by **R1** (black) and for the mutant enzyme (Tyr219Phe) modeled by **R3** (red).

RR and the first half of the TSR, therefore indicating that this contribution is not at all responsible for the different reaction barriers computed for **R1** and **R3**. This result is consistent with the results obtained by using the RFA in the sense that despite of the increase in the structural work observed after the mutation modeled by **R3**, it was finally concluded that the increase in the electronic reorganization led to the impairment of the enzyme, because this contribution was mostly affected.

The main reason behind the increased structural work on the mutant observed through the reaction force is actually related to the displacement of the TS towards a late stage of the reaction coordinate with respect to **R1**, which is easily identified through the ASM profile (i.e., the TS for **R3** is reached later than for **R1**). This means that when **R3** reaches a similar conformation as the one adopted by **R1** when entering to the TSR, **R3** is still required to continue with the structural deformation to enter into this region and reach the TS, as a consequence of the lower stabilization provided by ΔE_{int}. This observation is supported by the fact that the αC–F bond length of **R3** at the TS is 0.11 Å longer than **R1**, and the O···αC interaction distance needs to be 0.12 Å shorter in **R3** to reach the TS. Therefore, the main cause of the raise of the energy barrier after the mutation of Tyr219 comes from a less stabilizing interaction between the reactants of **R3** with respect to **R1** along the entire reaction coordinate (Figure 4a). This is indicative of a less favorable electronic process for **R3** during the reaction. To identify the source of the destabilization in the ΔE_{int} of the mutant enzyme, and thus of the electronic process involved, we performed EDA calculations along the reaction coordinate. As graphically shown in Figure 4b, the ΔE_{elstat} term becomes the main contributor to the total interaction energy from the reactants to the TSR. This is not surprising if we take into account the ionic nature of the reactants complex. Despite that, this electrostatic attraction is rather similar in both systems, and therefore is not the factor leading to the stronger interaction computed for **R1**. Instead, the orbital stabilization denoted by ΔE_{orb} is solely responsible for the higher ΔE_{int} computed for **R1** in going from the RR up to the corresponding TS. For instance, at the same C–F stretch of 0.3 Å, the difference in the orbital attractions $\Delta\Delta E_{orb} = 5.2$ kcal mol^{-1} roughly matches the total interaction energy difference between both transformations ($\Delta\Delta E_{int} = 5.0$ kcal mol^{-1}). This result reveals that the donor–acceptor interaction between the electron pair at Asp (donor fragment) and the vacant σ* molecular orbital from FAc moiety (acceptor) is stronger in **R1** than **R3**.

To integrate our findings regarding the effect of the mutation of the enzyme, we first have to consider that the chemical reaction taking place in **R1** and **R3** is exactly the same, in the sense that the nucleophile, electrophilic carbon, and leaving group are identical, with the only difference between **R1** and **R3** being the enzymatic environment, and more precisely, the environment of the fluorine atom. Then, the question to be answered is how the halogen pocket could possibly affect the O–αC bond formation process. To this end, we additionally studied the behavior of the electronic charge distribution between several fragments of our cluster models along the reaction coordinate. To our surprise, the results presented in Figure 5 showed that the central fragment of the reaction (H_2COO^-) exhibits similar magnitudes for the native and mutat-

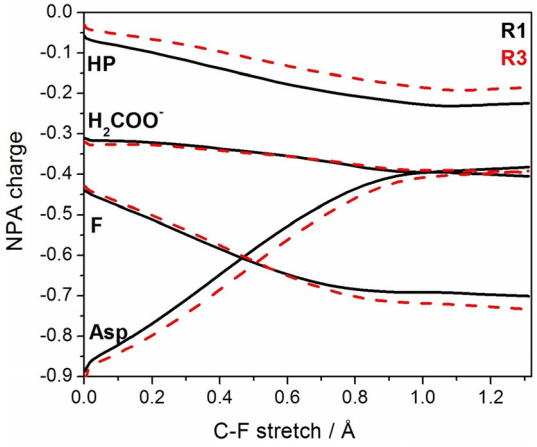

Figure 5. Electronic charge redistribution of key fragments from **R1** and **R3** (HP: halogen pocket; H_2COO^-: central moiety from FAc; F: fluorine; Asp: nucleophile). This allowed us to establish the differences in charge localization and transfer between the native enzyme (**R1**) and the mutant (**R3**). The variation of the charges during the reaction process was projected along the C–F stretch as reaction coordinate.

ed enzyme in the RR and up to the TS. On the other side, the fluorine atom also presented similar magnitudes between **R1** and **R3**. Remarkably, the main differences were localized between the halogen pocket and the nucleophile, which are placed at the two ends of the reaction axis connected by the αC–F bond. This interesting finding reveals that the electronic charge located in Asp is channeled through the S_N2 reaction axis, going from the nucleophilic oxygen, passing through the αC–F bond, and finally being received by the hydroxyl moiety from Tyr219. To sum up, the role of the Tyr219 in the reduction of the energy barrier is to decrease the electronic charge from the nucleophile, decreasing the Pauli repulsion between the reacting parts and thus, decreasing the energy demands to form the necessary donor–acceptor interaction derived from the electron pair at Asp (donor fragment) to the vacant σ* molecular orbital.

ASM-EDA for product stabilization: Effect of the mutant Tyr219Phe

As evident from the reaction energies, **R3** loses an important part of its ability to stabilize the product of the reaction, thus negatively affecting one of the main driving forces of the enzyme. From the ASM analysis in Figure 4a, it becomes evident that after the TS region, the ΔE_{strain} of **R3** starts to increase with respect to **R1**. This may be ascribed to the difficulties of the halogen pocket to accommodate the leaving group while it is actually dissociating from the αC. With respect to ΔE_{int}, after the TS, **R1** maintains its higher stability compared with **R3**, but without an appreciable increase in the ΔE_{int} difference between the native and the mutated enzyme. Hence, we suggest that the Tyr219Phe mutation impairs the ability of the catalytic site to aid in the proper accommodation of the forming products of the reaction. The EDA allowed us to properly understanding the electronic nature of this S_N2 reaction mechanism. An interesting feature of the mechanism is observed from Figure 4b, where ΔE_{orb} and ΔE_{Pauli} show a mirror-like behavior along the reaction coordinate. Meanwhile, the shape of the ΔE_{elstat} curve parallels that of the total interaction (ΔE_{int}), therefore confirming the major role of the electrostatic interactions in the process. After reaching the TS, **R1** presents an increase in ΔE_{Pauli}, which is then compensated by a slight increase in ΔE_{orb}, thus keeping the ΔE_{int} differences between **R1** and **R3**. After the ester bond is completely formed, the contribution of the ΔE_{orb} and ΔE_{elstat} terms to the total interaction is rather similar. Despite that, the main differences between **R1** and **R3** are still associated with the higher ΔE_{orb} stabilization, even though in the product state, **R1** presents slightly higher ΔE_{Pauli} repulsion. Thereby, our results rule out an electronic stabilization of the products, and strongly point towards a stabilization mechanism driven by the structural accommodation of the products of the reaction. Then, Tyr219 is essential to keep the proper architecture of the catalytic site, even more so than the His155 and Trp156.

Conclusions

In this work, we presented a detailed description of the inner workings of the catalytic machinery of defluorination through the comparison of the enzyme-catalyzed reaction with the previously reported non-catalyzed reaction in implicit solvent. The use of RFA showed the decrease of both structural and electronic work to achieve the $\Delta E^{\neq}$ reduction, and thus the catalysis of the reaction. Along with these findings, we provided a quantitative picture of each effect during the catalytic process. By means of the ASM-EDA method, the results from the RFA were complemented and a detailed picture of the physical factors governing the reduction of the $\Delta E^{\neq}$, and more importantly, of the mechanism by which the enzyme reduces the electronic work, is presented. By comparing the native form of the enzyme and a carefully selected mutant, which has been experimentally proven to impair the catalytic activity (namely the Tyr219Phe mutant), we found that the halogen pocket is able to act as a charge reservoir devoted to stabilizing the excess of charge involved in the reaction axis of the S_N2 reaction, mainly caused by Tyr219. Thus, the origin of the increase of the $\Delta E^{\neq}$ after the mutation is related to electronic more than structural grounds, which is also related to impairment of the TS stabilization carried out by the enzyme. Our results mark the relevance of the aromatic nature of the residues from the halogen pocket, a feature that may facilitate the process of accepting charge during the reaction. Another important finding was associated with the differences observed in the architecture of the halogen pocket of FAcD with respect to HAD enzymes. Here, the comparative analysis of the native and the mutant enzymes allowed us to observe that the removal of one of the anchoring points of fluorine, leading to a halogen pocket of two residues analogous to the HAD binding site, impairs the catalytic activity towards defluorination.

According to our results, we can conclude that the design of a mimetic with better performance should be first focused on the design of catalysts able to accommodate substrate and nucleophile in the reactive orientation, and secondly on providing an electronic charge reservoir linked to the leaving group, thus mimicking the role of the halogen pocket. This could be provided in heterogeneous catalysis by using a proper surface able to either attach the halogen through halogen bonds or to act as a charge acceptor favoring the nucleophilic attack as in the enzymatic context.

Computational Details

Conceptual background

Reaction force analysis (RFA): An elementary step of a chemical reaction is commonly described by the reactant(s), transition state, and product(s). However, much of the information necessary to rationalize the barrier height of a chemical reaction is hidden in the non-stationary states of a reaction. Through the calculation of the minimum energy path, it is possible to get these non-stationary states associated with the chemical reaction. With this at hand, a method to extract the

information is necessary. One method that has proven to be helpful in this sense is the so-called reaction force analysis (RFA). The reaction force corresponds to the negative derivative of the reaction energy with respect to the reaction coordinate (ξ) of the reaction,[21–23,27] and is expressed according to the following equation:

$$F(\xi) = -\frac{dE}{d\xi} \quad (1)$$

This simple expression provides the critical points along the reaction coordinate allowing us to separate it into three main regions as depicted in Figure 6. The first region, named the reactant region (RR), is comprehended from the reactant(s) (ξ_R) to the minimum in the reaction force profile (ξ_1). This is followed by the transition state region (TSR), which includes the transition state (TS) denoted by the point where the reaction force is equal to zero (ξ_{TS}), and continues until the maximum in the reaction force profile (ξ_2). Following the TSR is located the product region (PR), which goes from the maximum in the reaction force profile until the end of the reaction coordinate where the product or products are located (ξ_P).

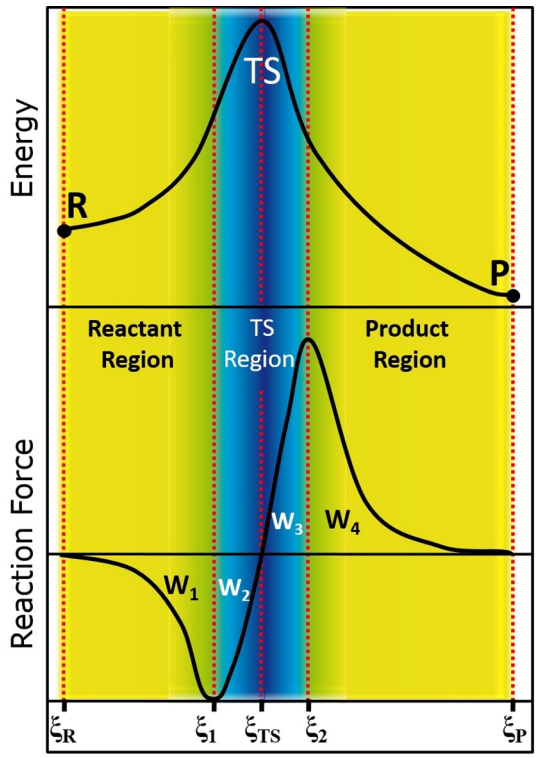

Figure 6. Schematic representation of a reaction energy profile for an exothermic reaction and its relationship with the reaction force profile and the reaction works. The regions dominated by structural work are denoted in yellow, whereas the region where the electronic work governs the progress of the reaction is represented in blue. It is assumed that in the point of the ξ between regions there is a combination of both components.

According to this scheme, it is possible to analyze the chemical reaction in terms of four reaction works (W_i):

$$W_1 = -\int_{\xi_R}^{\xi_1} F(\xi)d\xi > 0 \quad W_2 = -\int_{\xi_1}^{\xi_{TS}} F(\xi)d\xi > 0$$

$$W_3 = -\int_{\xi_{TS}}^{\xi_2} F(\xi)d\xi < 0 \quad W_4 = -\int_{\xi_2}^{\xi_P} F(\xi)d\xi < 0 \quad (2)$$

Each of these reaction works is dominated by particular factors that govern the progress of the reaction. A complete discussion about the definition and chemical interpretation of the reaction works is presented in the Supporting Information. The reaction work associated with the first region or RR, is quantified by the value of W_1 and is dominated by structural changes. Following along the reaction, the TSR is dominated by electronic work, where W_2 quantifies the energy necessary to reach the TS, whereas W_3 provides the magnitude associated with the electronic relaxation after crossing the TS. Once in the PR, the structural relaxation dominates the reaction progress, which is quantified by W_4. To sum up, the reaction works allow us to analyze the reaction mechanism in terms of structural and electronic factors, where the reaction energy (ΔE°) and the activation barrier ($\Delta E^{\neq}$) can be expressed according to the following equations:

$$\Delta E^0 = [E(\xi_P) - E(\xi_R)] = W_1 + W_2 + W_3 + W_4 \quad (3)$$

$$\Delta E^{\neq} = [E(\xi_{TS}) - E(\xi_R)] = W_1 + W_2 \quad (4)$$

Thus, the physical nature of the energy barrier can be described in terms of the relative weights of W_1 and W_2.

Activation strain model (ASM): Closely related to the RFA, the ASM of reactivity has become an extremely useful method to gain a quantitative understanding of what is behind a chemical reaction and to design more efficient chemical processes.[28–30] Here, we present the ASM analysis as a powerful approach to explore the mechanisms involved in the impairment of the enzymatic activity that results from the mutation of a residue from its binding site. We will use it to understand the effect of mutating the Tyr219 into phenylalanine. The ASM model is based on the decomposition of the potential energy surface into two main components that define the physical factors of a reaction:

$$\Delta E(\xi) = \Delta E_{strain}(\xi) + \Delta E_{int}(\xi_R) \quad (5)$$

Whereas the ΔE_{strain} term is the energy required to deform the individual reactants from their equilibrium geometries, the ΔE_{int} term measures the interaction between the deformed reactants as they approach each other. Then, monitoring ΔE_{int} along the reaction allows us to shed light on the source of the electronic activity quantified by the reaction work. The origin of the interactions involves different components without which it becomes difficult to really achieve a detailed rationalization of the process under study. For this, it is necessary to further decompose the interaction energy into contributions that can be more intuitive for a chemist to rationalize and use as a resource for the design of more efficient processes. To this end, the so-called energy decomposition analysis (EDA)

scheme[31,32] can be applied as it allows partitioning of the interaction energy into the following meaningful energy contributions:

$$\Delta E_{int}(\xi) = \Delta E_{orb}(\xi) + \Delta E_{elstat}(\xi) + \Delta E_{Pauli}(\xi) + \Delta E_{disp}(\xi) \quad (6)$$

Within this scheme, the orbital interaction (ΔE_{orb}) accounts for electron pair bonding, charge transfer, and polarization, the ΔE_{elstat} term corresponds to the classical coulombic/electrostatic attraction and repulsion between electrons and nuclei, the Pauli repulsion term (ΔE_{Pauli}) comprises the closed-shell repulsion between filled orbitals. Finally, the ΔE_{disp} term takes into account the interactions that result from dispersion forces. As a means to systematically identify the components that cause the energy barrier increase after mutating Tyr219 into phenylalanine, we used a fragmentation approach consisting of the nucleophile Asp110 together with the formamide moieties (oxyanion hole) as one fragment (Scheme 2; in green); and FAc, the anchoring arginines together with the halogen pocket as the other fragment (Scheme 2; in black). This scheme allowed us to isolate the structural and electronic components primarily associated with the O–αC bond formation process, and thus with respect to the reactant state.

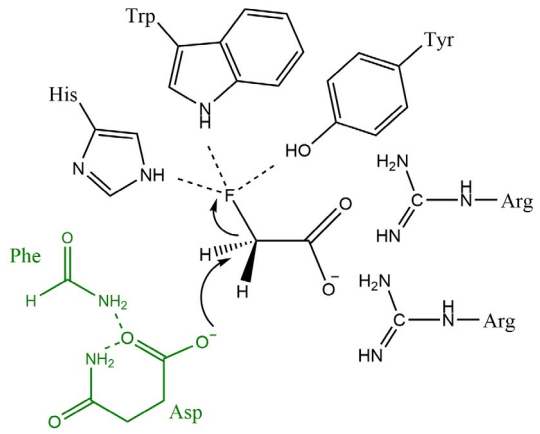

Scheme 2. Representation of the fragmentation scheme used to explore the effect in the reaction mechanism caused by the mutation of Tyr219 into phenylalanine. The first fragment (green) corresponds to the nucleophile with the oxyanion hole. The second fragment, (black) is constituted by the substrate, the halogen pocket, and the arginines in charge of anchoring the substrate.

Experimental Section

Preparation of starting geometries: The high-resolution crystal structure of bacterial FAcD (*Rhodopseudomonas palustris*) in complex with FAc was used as a starting point (PDB entry 3R3V), which was resolved to 1.5 Å.[9] The residue numbering used in this work follows that of the crystal structure. To capture the Michaelis complex, the aspartate in charge of the nucleophilic attack (Asp110) was mutated to asparagine, which was then manually modified back to aspartate to obtain a wild-type structure of FAcD. After visual inspection of this modified crystal structure, the Tyr219 residue from the halogen pocket was placed closer to the carboxylic acid of FAc (TyrO···O 2.74 Å) than to the halogen atom (TyrO···F 3.28 Å). Thereby, to evaluate the feasibility and stability of this conformation, the first step of this work consisted of running a short molecular dynamics (MD) calculation of 4 ns of the enzyme–substrate complex. For this purpose, we used VMD (v1.9.1)[33] to protonate and solvate the enzyme in a rectangular box of TIP3P water molecules. The most probable protonation states of the titratable residues were determined with PropKa,[34] considering a pH of 9.5 where the enzyme presents its highest proficiency. Ions were added to reach a concentration of 0.05 mol L^{-1} and to ensure charge neutrality of the system. The MD calculations were run with periodic boundary conditions by using the NAMD code version 2.9,[35] and the CHARMM22 force field.[36,37] The force field parameters for the substrate were obtained from homologous atoms in the CHARMM force field and the partial charges were calculated by the NPA method.[38] The time step was set to 2 fs and the Langevin piston Nosé–Hoover method[39] was used to keep the temperature and pressure at 300 K and 1 atm. The equilibration process consisted of four stages before the production dynamics. They first involved the relaxation of the water molecules while the protein was kept fixed through 2000 conjugate gradient steps and 0.1 ns of MD simulation. This was done to accommodate the water molecules located next to the cavities around the surface of the protein. Then, three subsequent MD calculations of 0.1 ns each were ran with a force constant restraint in the protein of 5.0, 2.0, and 0.1 kcal mol^{-1} $Å^{-2}$. Finally, a 4 ns MD calculation without restraint was performed and defined as our production trajectory.

Quantum chemical cluster models design: For our study, we selected the snapshot from the MD run with the closest geometry to the expected TS conformation, which involved a short distance between the nucleophile and the substrate, as well as short distances between the fluoride atom and the residues from the halogen pocket. The method for a rigorous snapshot selection and the proper number of structures needed for energy barrier determinations is still controversial. For example, in the work of Zhang and co-workers,[20] they used 20 snapshots per system. However, the snapshot selection involved taking random structures at intervals of 0.5 ns. This may lead to severe errors because some of these structures do not represent active or probable conformations that will actually contribute to the experimentally determined reaction barrier. Meanwhile, the conformations closer to the TS conformation are structures with the ability to pass through the reaction channel, leading to the best representation of the most probable reaction pathway. This point is supported by a very instructive article published by Fernandes et al.,[40] where they stated that only those conformations that coincide with possible reactant states close enough in energy to overcome the reaction barrier, defined by the potential energy landscape of the enzyme, will pass through the reaction channel. Therefore, it is expected that from a series of random reaction barriers, only those with low energy barriers will contribute with the experimental observations, as we proposed. Additionally, in a recent article from one of the authors of the present work,[41] it was proved that it is more relevant to choose a small number of snapshots that resemble the TS structure than selecting a large number of snapshots randomly. Careful selection of one snapshot will provide a proper structure for mechanistic studies, although not for an accurate quantification of the reaction barrier, which is not the goal of the present work. Here, we aim to take one of the most probable reaction pathways and to analyze in detail the inner structural and electronic phenomena taking place along the reaction for which there is no need to take more snapshots. After the snapshot selection, we designed a cluster model defined as **R1**, which represents the catalytic site in its wild type and therefore, constitutes our reference model. The

quantum chemical cluster approach has proven to be a powerful tool for the exploration of enzyme-catalyzed reactions with a high degree of accuracy, thus is our approach of choice for this study.[42,43] To understand the consequences of using the crystal structure conformation as a reference structure for computational studies, we designed the model **R2**. This allowed us to reveal the implications of using its coordinates for mechanistic exploration, also conveniently providing insight into the effect that the TyrOH···O interaction has on the barrier height and to determine whether it has a positive or negative role in the catalysis. **R1** and **R2** models included the His155, Trp156, and Tyr219 residues from the halogen pocket; Asp110 as the nucleophile; and the backbone atoms from Phe40 and Asp110 in the form of formamide molecules constituting the oxyanion hole. The latter residues were partially included because these interact with the non-nucleophilic oxygen from Asp110 helping the carboxylic acid to adopt a proper conformation for the nucleophilic attack. Arg111 and Arg114 were also included because these are in charge of anchoring the substrate to the catalytic site through the interaction between the carboxylic acid from FAc and the guanidinium group from the arginines. The final models for **R1** and **R2** consisted of 100 atoms. Considering that we performed intrinsic reaction coordinate (IRC) calculations with a large basis set, the size of the systems used in this work implied a high cost in terms of computational resources. To explore the mechanism by which the Tyr219Phe mutation disrupts the catalytic behavior, we designed a model representing the mutant form of the enzyme, defined as **R3**. To this end, we removed the hydroxyl group from Tyr219 obtaining the characteristic benzyl moiety from phenylalanine as the side chain. To systematically explore the functioning of the halogen pocket, and the architectural need of three residues instead of two as observed for HAD, we designed three additional models: one that lacks the His155 residue, one without the Trp156 residue, and a model without Tyr219, models defined as **R4**, **R5**, and **R6**, respectively. **R3**, **R4**, **R5**, and **R6** were built from **R1** and consisted of 99, 88, 81, and 84 atoms, respectively. However, after the optimization of the model without Tyr219 (**R6**), results shown in Figure S1 (in the Supporting Information), the model presented an artifact consisting of Arg111 interacting with the fluorine, an interaction that is not possible in the presence of Tyr219 because of spatial restrictions. This model does not accomplish the requirement of having two interacting points for the fluorine, and also includes an additional variable, that is, the effect of losing an anchoring point for the carboxylate from FAc, which is outside the scope of our study. Therefore, we only include a brief discussion of the results obtained from this model in the Supporting Information. Details about the procedure used to find the TSs and models truncation are presented in the Supporting Information. The polarizable continuum model (PCM) was used to consider the polarization caused by the enzyme environment with a dielectric constant set to 8.[44] Afterwards, we obtained the minimum energy path (MEP) connecting reactants, TS, and products by using the IRC approach.[45,46] All geometry optimizations and IRC calculations were carried out with Gaussian 09,[47] by using B3LYP[48,49] as the exchange-correlation functional and including the D3-dispersion correction developed by Grimme[50–52] as implemented in this software. The basis set used for production calculations was the 6-311 + g(d,p),[53] aiming to provide an acceptable accuracy for the energetics and to obtain a more appropriate description of the anions present in our systems. The ASM-EDA calculations were carried out with the ADF software,[54] by using a TZP basis set with the B3LYP density functional and incorporating the dispersion correction[50–52] as implemented in ADF, to keep consistency with the rest of the calculations. For these analyzes, we projected the energy profile and its contributions into the reaction coordinate associated with the αC–F bond stretching taking place during the reaction.

Acknowledgments

The authors are grateful for the financial support from FONDECYT through projects No. 3130383, 1140503, and 1130072. S.M.-R. is grateful for financial support from Grant ICM No 120082 and project DI-1323-16/R. I.F. is grateful for financial support from the Spanish MINECO-FEDER (Grants CTQ2016-78205-P and CTQ2014-51912-REDC).

Conflict of interest

The authors declare no conflict of interest.

Keywords: activation strain model · energy decomposition analysis · enzyme catalysis · reaction force

[1] C. Douvris, O. V. Ozerov, *Science* **2008**, *321*, 1188 – 1190.
[2] A. M. Calafat, L.-Y. Wong, Z. Kuklenyik, J. A. Reidy, L. L. Needham, *Environ. Health Perspect.* **2007**, *115*, 1596 – 1602.
[3] M. Houde, J. W. Martin, R. J. Letcher, K. R. Solomon, D. C. G. Muir, *Environ. Sci. Technol.* **2006**, *40*, 3463 – 3473.
[4] P. Goldman, *Science* **1969**, *164*, 1123 – 1130.
[5] R. A. Peters, *Adv. Enzymol. Relat. Areas Mol. Biol.* **1957**, *18*, 113 – 159.
[6] L. E. Twigg, R. W. Parker, *Anim. Welf.* **2010**, *19*, 249 – 263.
[7] E. K. A. Camboim, M. Z. Tadra-Sfeir, E. M. de Souza, F. de O. Pedrosa, P. P. Andrade, C. S. McSweeney, F. Riet-Correa, M. A. Melo, *Sci. World J.* **2012**, *2012*, 149893.
[8] P. Goldman, *J. Biol. Chem.* **1965**, *240*, 3434 – 3438.
[9] P. W. Y. Chan, A. F. Yakunin, E. A. Edwards, E. F. Pai, *J. Am. Chem. Soc.* **2011**, *133*, 7461 – 7468.
[10] K. Jitsumori, R. Omi, T. Kurihara, A. Kurata, H. Mihara, I. Miyahara, K. Hirotsu, N. Esaki, *J. Bacteriol.* **2009**, *191*, 2630 – 2637.
[11] A. Shurki, M. Štrajbl, J. Villa, A. Warshel, *J. Am. Chem. Soc.* **2002**, *124*, 4097 – 4107.
[12] M. H. M. Olsson, A. Warshel, *J. Am. Chem. Soc.* **2004**, *126*, 15167 – 15179.
[13] F. C. Lightstone, Y. J. Zheng, A. H. Maulitz, T. C. Bruice, *Proc. Natl. Acad. Sci. USA* **1997**, *94*, 8417 – 8420.
[14] F. C. Lightstone, Y.-J. Zheng, T. C. Bruice, *J. Am. Chem. Soc.* **1998**, *120*, 5611 – 5621.
[15] E. Y. Lau, K. Kahn, P. A. Bash, T. C. Bruice, *Proc. Natl. Acad. Sci. USA* **2000**, *97*, 9937 – 9942.
[16] S. K. Sadiq, P. V. Coveney, *J. Chem. Theory Comput.* **2015**, *11*, 316 – 324.
[17] K. E. Ranaghan, A. J. Mulholland, *Chem. Commun.* **2004**, 1238 – 1239.
[18] T. Kamachi, T. Nakayama, O. Shitamichi, K. Jitsumori, T. Kurihara, N. Esaki, K. Yoshizawa, *Chem. Eur. J.* **2009**, *15*, 7394 – 7403.
[19] T. Nakayama, T. Kamachi, K. Jitsumori, R. Omi, K. Hirotsu, N. Esaki, T. Kurihara, K. Yoshizawa, *Chem. Eur. J.* **2012**, *18*, 8392 – 8402.
[20] Y. Li, R. Zhang, L. Du, Q. Zhang, W. Wang, *Catal. Sci. Technol.* **2016**, *6*, 73 – 80.
[21] A. Toro-Labbé, *J. Phys. Chem. A* **1999**, *103*, 4398 – 4403.
[22] P. Politzer, J. V. Burda, M. C. Concha, P. Lane, J. S. Murray, *J. Phys. Chem. A* **2006**, *110*, 756 – 761.
[23] A. Toro-Labbé, S. Gutiérrez-Oliva, J. S. Murray, P. Politzer, *Mol. Phys.* **2007**, *105*, 2619 – 2625.
[24] A. P. Bento, M. Solà, F. M. Bickelhaupt, *J. Chem. Theory Comput.* **2008**, *4*, 929 – 940.
[25] Y. Zhao, D. G. Truhlar, *J. Chem. Theory Comput.* **2010**, *6*, 1104 – 1108.
[26] S. Miranda-Rojas, A. Toro-Labbé, *J. Chem. Phys.* **2015**, *142*, 194301.
[27] A. Toro-Labbé, S. Gutiérrez-Oliva, J. S. Murray, P. Politzer, *J. Mol. Model.* **2009**, *15*, 707 – 710.
[28] F. M. Bickelhaupt, *J. Comput. Chem.* **1999**, *20*, 114 – 128.

[29] W.-J. van Zeist, F. M. Bickelhaupt, *Org. Biomol. Chem.* **2010**, *8*, 3118 – 3127.
[30] I. Fernández, F. M. Bickelhaupt, *Chem. Soc. Rev.* **2014**, *43*, 4953 – 4967.
[31] T. Ziegler, A. Rauk, *Theor. Chim. Acta* **1977**, *46*, 1 – 10.
[32] F. M. Bickelhaupt, E. J. Baerends, *Rev. Comput. Chem.* **2007**, *15*, 1 – 86.
[33] W. Humphrey, A. Dalke, K. Schulten, *J. Mol. Graph.* **1996**, *14*, 33 – 38.
[34] M. H. M. Olsson, C. R. Søndergaard, M. Rostkowski, J. H. Jensen, *J. Chem. Theory Comput.* **2011**, *7*, 525 – 537.
[35] J. C. Phillips, R. Braun, W. Wang, J. Gumbart, E. Tajkhorshid, E. Villa, C. Chipot, R. D. Skeel, L. Kale, K. Schulten, *J. Comput. Chem.* **2005**, *26*, 1781 – 1802.
[36] A. D. MacKerell, D. Bashford, M. Bellott, R. L. Dunbrack, J. D. Evanseck, M. J. Field, S. Fischer, J. Gao, H. Guo, S. Ha, D. Joseph-McCarthy, L. Kuchnir, K. Kuczera, F. T. K. Lau, C. Mattos, S. Michnick, T. Ngo, D. T. Nguyen, B. Prodhom, W. E. Reiher, B. Roux, M. Schlenkrich, J. C. Smith, R. Stote, J. Straub, M. Watanabe, J. Wiórkiewicz-Kuczera, D. Yin, M. Karplus, *J. Phys. Chem. B* **1998**, *102*, 3586 – 3616.
[37] A. D. Mackerell, M. Feig, C. L. Brooks, *J. Comput. Chem.* **2004**, *25*, 1400 – 1415.
[38] A. E. Reed, R. B. Weinstock, F. Weinhold, *J. Chem. Phys.* **1985**, *83*, 735 – 746.
[39] S. E. Feller, Y. Zhang, R. W. Pastor, B. R. Brooks, *J. Chem. Phys.* **1995**, *103*, 4613 – 4621.
[40] A. J. M. Ribeiro, D. Santos-Martins, N. Russo, M. J. Ramos, P. A. Fernandes, *ACS Catal.* **2015**, *5*, 5617 – 5626.
[41] A. M. Cooper, J. Kästner, *ChemPhysChem* **2014**, *15*, 3264 – 3269.
[42] P. E. M. Siegbahn, F. Himo, *J. Biol. Inorg. Chem.* **2009**, *14*, 643 – 651.
[43] P. E. M. Siegbahn, F. Himo, *Wiley Interdiscip. Rev.: Comput. Mol. Sci.* **2011**, *1*, 323 – 336.
[44] M. R. A. Blomberg, T. Borowski, F. Himo, R.-Z. Liao, P. E. M. Siegbahn, *Chem. Rev.* **2014**, *114*, 3601 – 3658.
[45] K. Fukui, *Acc. Chem. Res.* **1981**, *14*, 363 – 368.
[46] C. Gonzalez, H. B. Schlegel, *J. Phys. Chem.* **1990**, *94*, 5523 – 5527.
[47] Gaussian 09, Revision B.01, M. J. Frisch, G. W. Trucks, H. B. Schlegel, G. E. Scuseria, M. A. Robb, J. R. Cheeseman, G. Scalmani, V. Barone, B. Mennucci, G. A. Petersson, H. Nakatsuji, M. Caricato, X. Li, H. P. Hratchian, A. F. Izmaylov, J. Bloino, G. Zheng, J. L. Sonnenberg, M. Hada, M. Ehara, K. Toyota, R. Fukuda, J. Hasegawa, M. Ishida, T. Nakajima, Y. Honda, O. Kitao, H. Nakai, T. Vreven, J. A. Montgomery, Jr., J. E. Peralta, F. Ogliaro, M. Bearpark, J. J. Heyd, E. Brothers, K. N. Kudin, V. N. Staroverov, R. Kobayashi, J. Normand, K. Raghavachari, A. Rendell, J. C. Burant, S. S. Iyengar, J. Tomasi, M. Cossi, N. Rega, J. M. Millam, M. Klene, J. E. Knox, J. B. Cross, V. Bakken, C. Adamo, J. Jaramillo, R. Gomperts, R. E. Stratmann, O. Yazyev, A. J. Austin, R. Cammi, C. Pomelli, J. W. Ochterski, R. L. Martin, K. Morokuma, V. G. Zakrzewski, G. A. Voth, P. Salvador, J. J. Dannenberg, S. Dapprich, A. D. Daniels, Ö. Farkas, J. B. Foresman, J. V. Ortiz, J. Cioslowski, D. J. Fox, Gaussian, Inc. Wallingford CT, **2009**.
[48] A. D. Becke, *J. Chem. Phys.* **1993**, *98*, 5648 – 5652.
[49] C. Lee, W. Yang, R. G. Parr, *Phys. Rev. B* **1988**, *37*, 785 – 789.
[50] S. Grimme, *J. Comput. Chem.* **2004**, *25*, 1463 – 1473.
[51] S. Grimme, *J. Comput. Chem.* **2006**, *27*, 1787 – 1799.
[52] S. Grimme, J. Antony, S. Ehrlich, H. Krieg, *J. Chem. Phys.* **2010**, *132*, 154104.
[53] M. J. Frisch, J. A. Pople, J. S. Binkley, *J. Chem. Phys.* **1984**, *80*, 3265 – 3269.
[54] G. te Velde, F. M. Bickelhaupt, E. J. Baerends, C. Fonseca Guerra, S. J. A. van Gisbergen, J. G. Snijders, T. Ziegler, *J. Comput. Chem.* **2001**, *22*, 931 – 967.

Manuscript received: September 19, 2017
Revised manuscript received: October 26, 2017
Accepted manuscript online: November 2, 2017
Version of record online: January 29, 2018